

# Contact Dynamic Models of Space Debris Capturing Using A Net

Minghe Shan\*<sup>‡</sup>, Jian Guo\* and Eberhard Gill\*

\* Faculty of Aerospace Engineering, Delft University of Technology  
Kluyverweg 1, 2629 HS, Delft, The Netherlands

m.shan@tudelft.nl · j.guo@tudelft.nl · e.k.a.gill@tudelft.nl

<sup>‡</sup>Corresponding author

## Abstract

Contact dynamic models for active debris removal using a net are presented and analysed using numerical simulations. The contact dynamics are based on two methods: the penalty-based method and the impulse-based method. Both methods apply contact detection algorithm based on Axis-Aligned Bounding Box (AABB). The impulse-based method is, for the first time, being used in the net capturing scenario. Strengths and weaknesses of these two contact dynamic models are compared and discussed. Moreover, the results from numerical simulations of target capturing are presented and analyzed to evaluate the effectiveness of the contact dynamic models.

## 1. Introduction

Space debris is a serious threat to existing and future space missions. Many space debris capturing and removal methods have been proposed and investigated to mitigate this risk.<sup>5</sup> One of the most promising methods of space debris removal is net capturing which has been discussed widely. The Robotic Geostationary Orbit Restorer (ROGER) is the first project that proposed the net capturing method. Its objective is to transport a target into a graveyard orbit using a net.<sup>2</sup> The net capture mechanism consists of four flying weights in each corner of a squared net. The flying weight is called "bullet", shot by a spring system, named net gun. These four bullets help expand the large net thus wrapping a target up.

The process of space debris capturing with a net includes, net deployment, target capturing and de-orbiting. Net deployment analysis is referred to the reference [6].<sup>6</sup> This paper focuses on the second step, target capturing, especially the contact dynamics between the net and the target. The contact modeling methods commonly used are penalty-based method and impulse-based method. For the penalty-based method, it is not difficult to be implemented either in programming or in theoretical derivation. In Botta's<sup>3</sup> and Benvenuto's<sup>1</sup> work, they both use the penalty-based method to evaluate the contact force between the net and the target. However, in the penalty-based method, a large contact stiffness is needed to keep the penetration sufficiently small that will generate large forces leading to stiff equation system. Moreover, a contact stiffness suitable for one situation is not necessarily proper for another. For the impulse-based method, it has always been used in game environment and/or virtual reality environment. Furthermore, it has always been used in the contact between two separate bodies.<sup>4</sup> In this paper, the impulse-based method as a contact modeling method is, for the first time, being used in the net capturing scenario. Specially, in the net capturing situation, the capture is regarded as multiple bodies contact with one single object. Theoretical solutions for this special situation is derived in this paper, and simulation of a Envisat mock-up capturing based on the impulse-based method is performed and compared with that of the penalty-based method.

This paper is organized into six sections. The mathematic model of a space tethered-net established based on the mass-spring method is described in Section 2. In Section 3, contact detection algorithm and two contact dynamic models are presented in detail. Simulations based on the mass-spring model and two contact dynamic models are described in Section 4. Moreover, Section 5 compares the two contact modeling methods and characterizes them. Section 6 provides conclusions.

## CONTACT DYNAMIC MODELS OF SPACE DEBRIS CAPTURING USING A NET

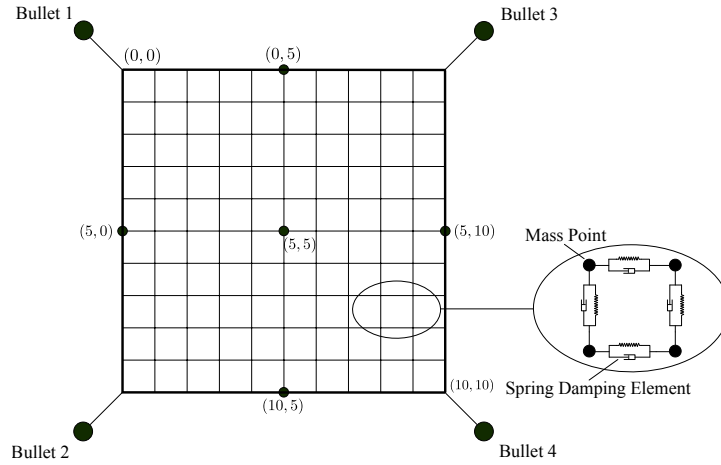


Figure 1: Geometrical and physical configuration of a net.

## 2. Dynamic Model of a Net

In this section, the dynamic modeling of a net is established based on a mass-spring model. A mass-spring model approximates a flexible cable as a series of mass points connected by mass-less spring-damper elements. The geometrical and physical configuration of the net is shown in Fig. 1. Four bullets are attached at the corners of the net with additional cables. The mass points of the net are numbered sequentially as a matrix as shown in Fig. 1. According to the nature of the cable material, cable elements are not able to withstand compression and a tension force will only be generated when the cables are elongated. Based on the linear Kelvin-Voigt model, the tension force  $\mathbf{f}_{ij}$  between nodes  $i$  and  $j$  can be expressed as

$$\mathbf{f}_{ij} = \begin{cases} f_{ij}\hat{\mathbf{r}}_{ij} & r_{ij} > l_0 \text{ and } \dot{f}_{ij} < 0, \\ 0 & r_{ij} \leq l_0 \text{ or } \dot{f}_{ij} > 0, \end{cases} \quad (1)$$

where  $f_{ij} = -k(r_{ij} - l_0) - c\dot{r}_{ij}$ . In this equation,  $r_{ij}$  and  $\dot{r}_{ij}$  are the distance and the relative velocity between the  $i$ -th and  $j$ -th node. Further,  $\hat{\mathbf{r}}_{ij}$  represents the unit direction vector along the  $i$ -th and  $j$ -th node expressed in the local reference frame. The axial stiffness  $k$  of the cable is defined as  $k = EA/l_0$ , in which  $E$  is the elastic Young's modulus of cable material,  $A$  the cross section of the cable and  $l_0$  the initial un-stretched mesh length. The damping coefficient  $c$  of the cable material depends on the cable mass and cable stiffness with its damping ratio  $\xi$ , according to  $c_i = 2\xi\sqrt{m_i k}$ .

The chaser satellite is assumed to be approached along track with the target before shooting the net. The absolute position of mass points in the inertial reference frame is expressed as  $\mathbf{r}_i^e = \mathbf{r}_p + \mathbf{R}^o \mathbf{r}_i$ , in which  $\mathbf{r}_i^e$  is the absolute position vector of the  $i$ -th node in the inertial frame, and  $\mathbf{R}^o$  is the rotation matrix that transforms the position vector  $\mathbf{r}_i$  from the local frame to the inertial frame. With such a model, the dynamic equations of motion for the entire net can be discretized as

$$m_i \frac{d\mathbf{r}_i^e}{dt} = \sum_{j=1}^{N_i} \mathbf{R}^o \mathbf{f}_{ij} + \sum_{s=1}^{M_i} \mathbf{f}_{is}^e + \mathbf{g}_i, \quad (2)$$

where  $N_i$  is the number of adjacent cables connected to the  $i$ -th node,  $\mathbf{f}_{ij}$  is the force on the  $i$ -th node generated by the  $j$ -th cable connected to it,  $M_i$  is the number of external forces on the  $i$ -th node, and  $\mathbf{f}_{is}^e$  is the sum of external forces, e.g., aerodynamic drag, solar radiation pressure and other perturbations. The micro-gravitational force  $\mathbf{g}_i$  on the  $i$ -th node is given by  $\mathbf{g}_i = -\mu_g M m_i \mathbf{r}_i^e / |\mathbf{r}_i^e|^3$ , in which  $\mu_g$  is the universal gravitational constant,  $M$  the mass of the Earth.

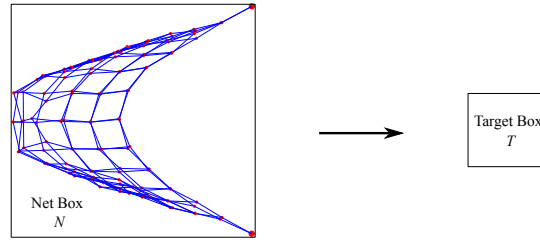
## 3. Contact Dynamic Models

In this section, the contact detection algorithm and two contact dynamic models are presented.

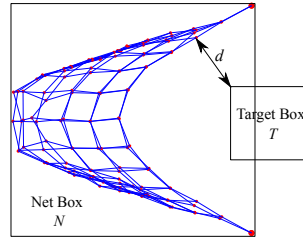
### 3.1 Contact Detection

Contact detection needs to be performed at every step of the simulation. In this paper, the contact detection, based on Axis-Aligned Bounding Box (AABB) method, is divided into two levels so as to improve the computational performance of the simulation. In the first level detection, the net and the target are assumed to be contained in the box  $N$  and

## CONTACT DYNAMIC MODELS OF SPACE DEBRIS CAPTURING USING A NET



(a) Net approaching the target (First level detection)



(b) Two boxes intersect (Second level detection)

Figure 2: Contact detection.

the box  $T$ , respectively. Therefore, the first level contact detection is only performed between these two boxes. The second level contact detection starts once the two boxes intersect with each other. In the second level detection, every node of the net is checked by calculating the distance  $d$  between the node and the target. Once the distance is smaller than a threshold distance  $\epsilon$ , respective contact response will be applied on the node. The contact response is dependent on the chosen contact modeling method, namely, penalty-based method or impulse-based method.

### 3.2 Penalty-Based Method

In the penalty-based method, the response force is dependent on the penetration. The larger the penetration, the higher the penalty.

#### 3.2.1 Normal contact force

Spring-dashpot model is being used to evaluate the normal contact force between objects. The normal force  $f_n$  is dependent on the penetration depth  $\delta$  and the penetration rate  $\dot{\delta}$  in the penalty based method, which is expressed as

$$f_n = k\delta + d\dot{\delta}, \quad (3)$$

where  $k$  is the contact stiffness and  $d$  is the damping coefficient.

For the aforementioned net model, net is modeled by a series of connected mass points. The contact of the mass point with the surface of the target is regarded as a sphere-plane contact. According to the Hertzian contact theory, for a sphere-plane contact, contact stiffness can be obtained by

$$k = \frac{4\sqrt{r}}{3\pi(h_1 + h_2)}, \quad (4)$$

with

$$h_i = \frac{1 - \nu_i^2}{\pi E_i}, \quad (i = 1, 2), \quad (5)$$

where  $E_i$  and  $\nu_i$  are Young's modulus and Poisson's ratio of the material of the contacting bodies, and  $r$  is the radius of the contact mass point.

The damping coefficient  $d$  is expressed as,

$$d = 2\xi\sqrt{km}, \quad (6)$$

with  $\xi$  the damping ratio, and  $m$  the mass of the contacting node.

### 3.2.2 Friction

Frictional force vector generated from the contact is always opposite to the relative velocity along the tangential direction of the contact surface. Assume a mass point  $p_i$  contact with a object on point  $O$ , and the normal vector of point  $O$  on the object is  $\mathbf{n}$ , Then the relative velocity  $\mathbf{v}_r$  of the points  $p_i$  and  $O$  is

$$\mathbf{v}_r = \mathbf{v}_{p_i} - \mathbf{v}_O. \quad (7)$$

The component of the relative velocity along the normal is

$$\mathbf{v}_{Nr} = (\mathbf{n}' \mathbf{v}_r) \mathbf{n}. \quad (8)$$

Therefore, the relative velocity along the tangential direction is obtained

$$\mathbf{v}_t = \mathbf{v}_r - \mathbf{v}_{Nr}. \quad (9)$$

According to the Coulomb's law of friction, the friction can be expressed as

$$\mathbf{f}_t = \mu f_n \mathbf{n}_t, \quad (10)$$

with  $\mathbf{n}_t = \mathbf{v}_t / v_t$ , and  $\mu$  is the Coulomb's friction coefficient.

### 3.3 Impulse-Based Method

In the impulse-based method, the impulse caused by the contact, instead of the contact force, is calculated and therefore the velocity change after contact can be computed. Introducing the coefficient of restitution  $e$ , the relative velocity change can be expressed as

$$e = -\frac{v_r^+}{v_r^-}, \quad (11)$$

where  $0 \leq e \leq 1$ . In this paper, superscript '-' and '+' indicate the status before and after the contact. Thus,  $v_r^+$  is the relative velocity of two objects after the contact, and  $v_r^-$  is the relative velocity of two objects before the contact. When  $e = 0$ , then  $v_r^+ = 0$ , the contact is fully inelastic contact. When  $e = 1$ ,  $v_r^+ = -v_r^-$ , the contact is fully elastic contact.

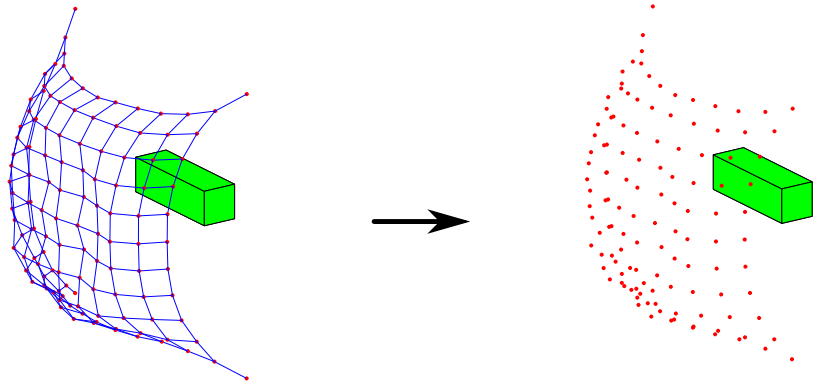


Figure 3: Net contact with a target

As shown in Fig. 3, a net contact with a target can be regarded as multiple mass points with one single object. Imagine that  $n$  mass points contact with an object  $O$ . Velocities of  $n$  mass points and the object  $O$  are represented by  $\mathbf{v}_i$  and  $\mathbf{v}_O$ , respectively. Angular velocity of the object  $O$  is  $\omega_O$ . Let  $\mathbf{n}_i$  represent the normal direction of the contact plane,  $m_i$  represent the mass of  $i$ -th contact point, and  $j_i$  represent the magnitude of the impulse of  $i$ -th contact. Therefore, the velocities of mass points after contact are

$$\begin{aligned} \mathbf{v}_1^+ &= \mathbf{v}_1^- + j_1 \mathbf{n}_1 / m_1 \\ \mathbf{v}_2^+ &= \mathbf{v}_2^- + j_2 \mathbf{n}_2 / m_2 \\ &\dots \\ \mathbf{v}_n^+ &= \mathbf{v}_n^- + j_n \mathbf{n}_n / m_n. \end{aligned} \quad (12)$$

The linear and angular velocity of the target after contact are,

$$\begin{aligned} \mathbf{v}_O^+ &= \mathbf{v}_O^- - (j_1 \mathbf{n}_1 + j_2 \mathbf{n}_2 + \dots + j_n \mathbf{n}_n) / m_O \\ \omega_O^+ &= \omega_O^- - \mathbf{I}_O^{-1} (\mathbf{r}_1 \times j_1 \mathbf{n}_1 + \mathbf{r}_2 \times j_2 \mathbf{n}_2 + \dots + \mathbf{r}_n \times j_n \mathbf{n}_n). \end{aligned} \quad (13)$$

In the above equation, contact impulse vector  $\mathbf{j}$  is an undetermined vector,

$$\mathbf{j} = [j_1, j_2, \dots, j_n]^T. \quad (14)$$

In order to simplify the expression, here we define the normal vector  $\mathbf{N}$  as

$$\mathbf{N} = [\mathbf{n}_1, \mathbf{n}_2, \dots, \mathbf{n}_n]^T, \quad (15)$$

and  $\Sigma \mathbf{r} \mathbf{n}$  is defined as the following expression

$$\Sigma \mathbf{r} \mathbf{n} = \sum_{i=1}^{i=n} \mathbf{r}_i \times j_i \mathbf{n}_i. \quad (16)$$

Therefore, Eq. 13 is simplified as,

$$\begin{aligned} \mathbf{v}_O^+ &= \mathbf{v}_O^- - \mathbf{N}^T \mathbf{j} / m_O \\ \boldsymbol{\omega}_O^+ &= \boldsymbol{\omega}_O^- - \mathbf{I}_O^{-1} \Sigma \mathbf{r} \mathbf{n}. \end{aligned} \quad (17)$$

Based on the impulse conservation law and introducing the coefficient of restitution  $e$ , relative velocities after contact in the direction normal to the contact plane can be derived as

$$\begin{aligned} -(e+1)v_{r1}^- &= \mathbf{n}_1 [j_1 \mathbf{n}_1 / m_1 + \mathbf{N}^T \mathbf{j} / m_O + (\mathbf{I}_O^{-1} \Sigma \mathbf{r} \mathbf{n}) \times \mathbf{r}_1] \\ -(e+1)v_{r2}^- &= \mathbf{n}_2 [j_2 \mathbf{n}_2 / m_2 + \mathbf{N}^T \mathbf{j} / m_O + (\mathbf{I}_O^{-1} \Sigma \mathbf{r} \mathbf{n}) \times \mathbf{r}_2] \\ &\dots \\ -(e+1)v_{rn}^- &= \mathbf{n}_n [j_n \mathbf{n}_n / m_n + \mathbf{N}^T \mathbf{j} / m_O + (\mathbf{I}_O^{-1} \Sigma \mathbf{r} \mathbf{n}) \times \mathbf{r}_n]. \end{aligned} \quad (18)$$

On left side, the expression can be simplified as a vector notation  $\mathbf{v}$ ,

$$\mathbf{v} = -(e+1)[v_{r1}^-, v_{r2}^-, \dots, v_{rn}^-]^T. \quad (19)$$

To simplify the expression of Eq. 18, in this paper, we define

$$\mathbf{IC}_{ijk} = (\mathbf{I}_O^{-1} (\mathbf{r}_i \times \mathbf{n}_j)) \times \mathbf{r}_k. \quad (20)$$

Thus, the coefficient matrix is derived from Eq. 18,

$$\mathbf{M} = \begin{bmatrix} \frac{1}{m_1} + \frac{1}{m_O} + \mathbf{n}_1 \mathbf{IC}_{111} & \frac{\mathbf{n}_1 \mathbf{n}_2}{m_O} + \mathbf{n}_1 \mathbf{IC}_{221} & \dots & \frac{\mathbf{n}_1 \mathbf{n}_n}{m_O} + \mathbf{n}_1 \mathbf{IC}_{nn1} \\ \frac{\mathbf{n}_2 \mathbf{n}_1}{m_O} + \mathbf{n}_2 \mathbf{IC}_{112} & \frac{1}{m_2} + \frac{1}{m_O} + \mathbf{n}_2 \mathbf{IC}_{222} & \dots & \frac{\mathbf{n}_2 \mathbf{n}_n}{m_O} + \mathbf{n}_2 \mathbf{IC}_{nn2} \\ \vdots & \vdots & \ddots & \vdots \\ \frac{\mathbf{n}_n \mathbf{n}_1}{m_O} + \mathbf{n}_n \mathbf{IC}_{11n} & \dots & \dots & \frac{1}{m_n} + \frac{1}{m_O} + \mathbf{n}_n \mathbf{IC}_{nnn} \end{bmatrix}. \quad (21)$$

Equation 18 is written as,

$$\mathbf{M} \mathbf{j} = \mathbf{v}. \quad (22)$$

Therefore, the magnitude of the impulse of every contact is easily computed by,

$$\mathbf{j} = \mathbf{M}^{-1} \mathbf{v}. \quad (23)$$

With a computed  $\mathbf{j}$ , the velocities after contact can consequently be achieved by Eq. 12 and 13.

## 4. Simulations

In this section, simulations of a fixed Envisat mock-up capturing are performed based on the penalty-based method and the impulse-based method, respectively, to evaluate the effectiveness of the contact dynamic models. Two case studies have been performed with different parameters. The simulation parameters of the net and the target information are summarised in Table. 1.

Net capturing process can be divided into three steps: net deployed, net approaches to the target and target capturing. Contact detection introduced above is performed at every step of the simulation. Contact response is achieved based on the chosen contact model, the penalty-based method or the impulse-based method. Figure 4 shows the simulation of the net capturing process by the penalty-based method and Fig. 5 shows the simulation of the capturing by the impulse-based method. Both of them are under parameters of the first case study. It is noticed that the configurations of the net are always close to each other. This indicates that the contact responses, either contact force or contact impulse, both are able to describe the multiple contacts dynamics.

## CONTACT DYNAMIC MODELS OF SPACE DEBRIS CAPTURING USING A NET

Table 1: Simulation Parameters

Parameters	Case 1	Case 2
Net size $A$ , [m <sup>2</sup> ]	0.8×0.8	0.8×0.8
Mesh length $l_0$ , [m]	0.08	0.08
Cable diameter $d$ , [mm]	1	1
Edge cable diameter $d_e$ , [mm]	3	3
Bullet mass $m_b$ , [kg]	0.03×4	0.05×4
Material elastic modulus $E$ , [Pa]	4.456×10 <sup>8</sup>	4.456×10 <sup>8</sup>
Shooting velocity $v$ , [m/s]	1.8	1.5
Shooting angle $\theta$ , [deg]	25	30
Simulation time $t$ , [s]	3	3

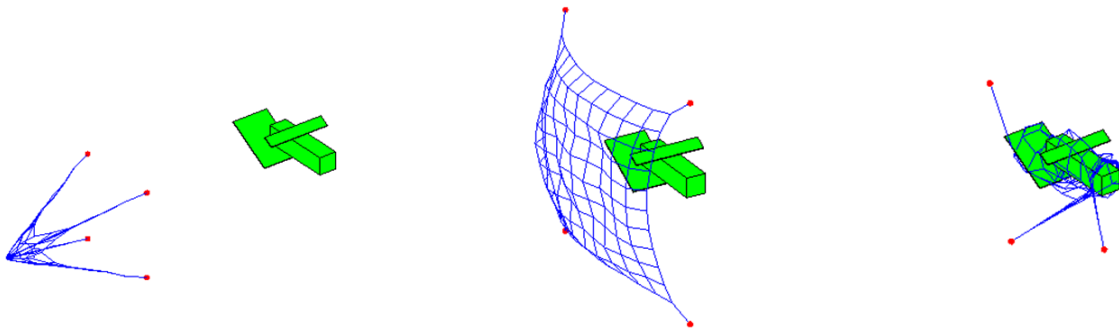


Figure 4: Envisat Mockup Capturing (Penalty-based Method)

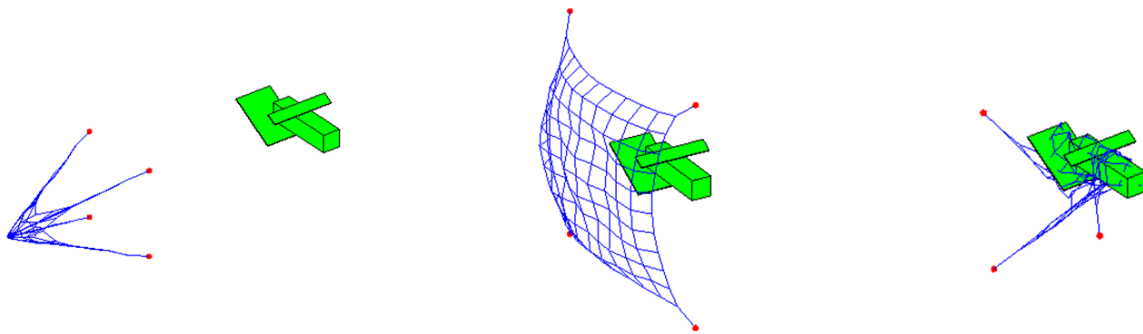


Figure 5: Envisat Mockup Capturing (Impulse-based Method)

## 5. Comparison, Analysis and Discussion

The main difference of the two contact dynamic models, the penalty-based method and the impulse-based method, is the way of coping with the contact response. For the penalty-based method, the contact response is the contact force which is dependent on the penetration. On the contrary, for the impulse-based method, the contact response is based on the impulse from the impact. As introduced in the above section, in the first case of Envisat mock-up capturing based on these two contact modeling methods, maximum contact force obtained from the penalty-based method, and maximum contact impulse obtained from the impulse method is achieved as shown in Fig. 6 and 7, respectively. From which, we figured that at time 0.9 s, the net starts to contact with the target. The maximum contact force is less than 6 N, and the maximum impulse is less than  $5 \times 10^{-4}$  Ns. It is worth mentioning that not all the results from the second case study are included in this paper due to requirements of compactness, concision and a page limit.

To further quantitatively analyze the difference of two contact models, the trajectories of bullets are plotted and presented in Fig. 8. From which, it is noticed that the trajectories of bullets obtained from these two contact dynamic models are quite close to each other. The displacement difference of the bullets trajectories under two case studies are

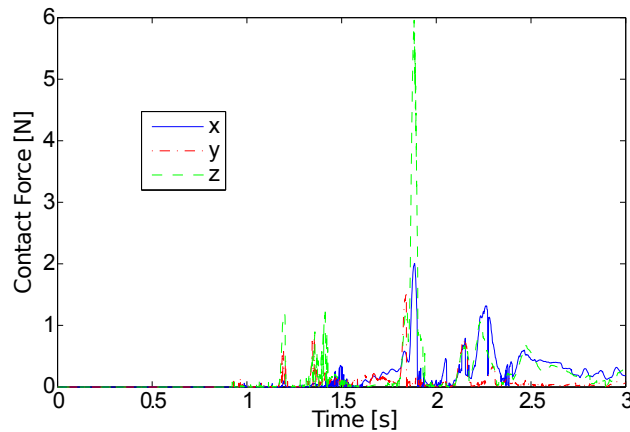


Figure 6: Maximum Contact Force (Penalty-based Method)

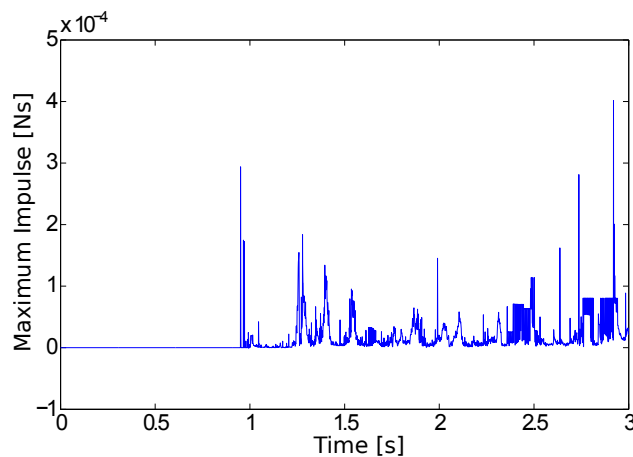


Figure 7: Maximum Impulse (Impulse-based Method)

shown in Fig. 9. The largest difference in the first case comes from bullet 2 along  $x$  direction, which is within 0.35 m. However, the average difference is small as 5.26 cm. In the second case study with initial parameters shown in Table. 1, the largest difference and the average difference computed are even smaller, which are 0.24 m and 4.38 cm, respectively.

In these two contact modeling methods, it is not that one method is better than the other one in any case. Each method has its own strength and weakness. For instance, for the penalty-based method, the contact force can be easily achieved and it is good at coping with the simultaneous contacts, either from a programming point of view or from a theoretical point of view. However, in the penalty-based method, a large contact stiffness is needed to keep the penetration sufficiently small that will generate large forces leading to stiff equation system. On the contrary, impulse-based method can avoid the penetration and the stiff equations system. However, it requires a smaller step size when dealing with a small coefficient of restitution. In addition, when it comes to the simultaneous contacts, the impulse-based method is not as handy as the penalty-based method. In Table. 2, these two contact modeling methods are compared from different aspects.

## 6. Conclusion

In this paper, two contact modeling methods: the penalty-based method and the impulse-based method are presented. Simulations of a fixed Envisat mock-up capturing with different parameters based on these two methods have been performed. The results of the numerical simulations of target capturing are analyzed to evaluate the effectiveness of the contact dynamic models. The average differences of two cases simulation results based on two contact modeling methods is small as 5.26 cm and 4.38 cm. In addition, strengths and weaknesses of these two contact dynamic models are compared in different aspects.

CONTACT DYNAMIC MODELS OF SPACE DEBRIS CAPTURING USING A NET

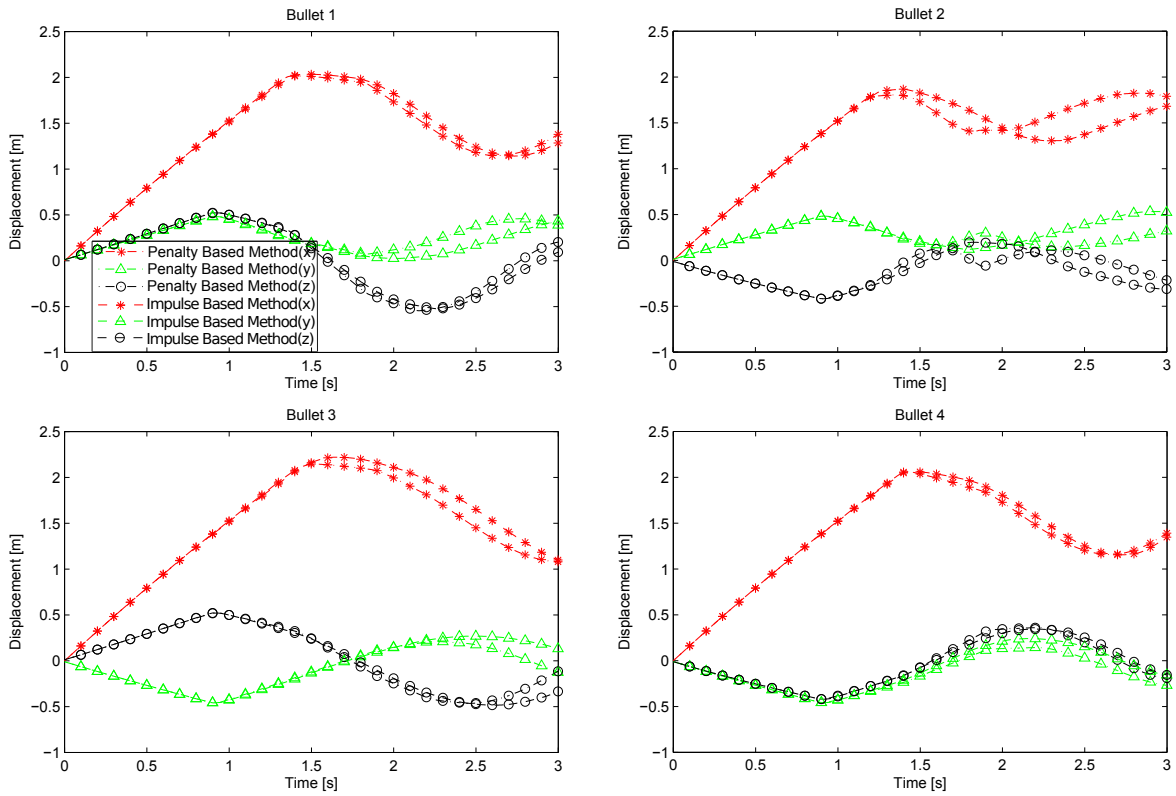


Figure 8: Comparison of two contact dynamic methods

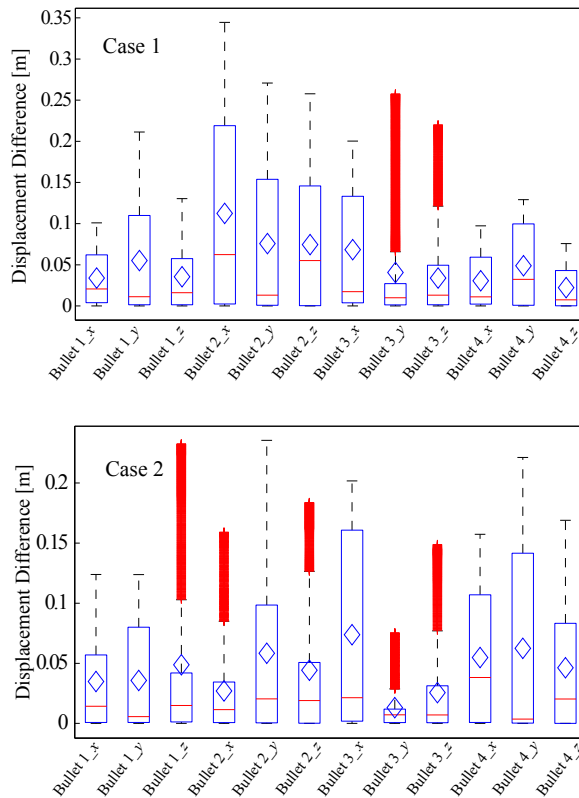


Figure 9: Displacement difference of the bullets with boxplot

Table 2: Comparison of Two Contact Dynamic Models

	Penalty-based Method	Impulse-based Method
Contact Response	Explicit contact force based on penetration	Collision impulse applied on contact bodies
Penetration	Yes	No
Differential equations	Stiff when penalty is high	Non-stiff
Computational robustness	Fair	Good
Step size	Fair	Small
Handling of simultaneous contacts	Good	Fair

## Acknowledgments

The first author, Minghe Shan, acknowledges the financial support from the Chinese Scholarship Council for PhD Scholarship.

## References

- [1] Riccardo Benvenuto, Michèle Lavagna, and Samuele Salvi. Multibody dynamics driving gnc and system design in tethered nets for active debris removal. *Advances in Space Research*, 58(1):45–63, 2016.
- [2] Bernd Bischof, L Kerstein, J Starke, H Guenther, W Foth, et al. Roger-robotic geostationary orbit restorer. In *54th International Astronautical Congress of the International Astronautical Federation, the International Academy of Astronautics, and the International Institute of Space Law*, pages IAA–5. 2003.
- [3] Eleonora M Botta, Inna Sharf, and Arun K Misra. Contact dynamics modeling and simulation of tether nets for space-debris capture. *Journal of Guidance, Control, and Dynamics*, pages 1–14, 2016.
- [4] Brian Vincent Mirtich. *Impulse-based dynamic simulation of rigid body systems*. PhD thesis, University of California at Berkeley, 1996.
- [5] Minghe Shan, Jian Guo, and Eberhard Gill. Review and comparison of active space debris capturing and removal methods. *Progress in Aerospace Sciences*, 80:18–32, 2016.
- [6] Minghe Shan, Jian Guo, and Eberhard Gill. Deployment dynamics of tethered-net for space debris removal. *Acta Astronautica*, 132:293–302, 2017.